Supplementary Information

Biphasic growth dynamics during *Caulobacter crescentus* division

Shiladitya Banerjee,[1,2,3] Klevin Lo,[1,4] Matthew K. Daddysman,[4] Alan Selewa,[4,5] Thomas Kuntz,[6] Aaron R. Dinner,[1,4,6,†] and Norbert F. Scherer[1,4,6,†]

[1] *James Franck Institute, The University of Chicago, Chicago IL 60637, USA*

[2] *Department of Physics and Astronomy, University College London, London WC1E 6BT, UK*

[3] *Institute for the Physics of Living Systems, University College London, London WC1E 6BT, UK*

[4] *Institute for Biophysical Dynamics, The University of Chicago, Chicago IL 60637, USA*

[5] *Biophysical Sciences Graduate Program, The University of Chicago, Chicago IL 60637, USA*

[6] *Department of Chemistry, The University of Chicago, Chicago IL 60637, USA*

Supplementary Methods

Acquisition of Experimental Data. As described in [1, 2], the inducibly-sticky *Caulobacter crescentus* strain FC1428 was introduced into a microfluidic device and cells were incubated for one hour in the presence of the vanillate inducer. The device was placed inside a homemade acrylic microscope enclosure ($39'' \times 28'' \times 27''$) equilibrated to 31°C (temperature controller: CSC32J, Omega and heater fan: HGL419, Omega) and at other temperatures (see Supplementary Figure 2). At the start of the experiment, complex medium (peptone-yeast extract; PYE) was infused through the channel at a constant flow rate of 7 μL/min using a synringe pump (PHD2000, Harvard Apparatus), which flushed out non-adherent cells. A microscope (Nikon Ti Eclipse with perfect focus system) and robotic XY stage (Prior Scientific ProScan III) under computerized control (LabView 8.6, National Instrument) were used to acquire phase-contrast images at a magnification of 250X (EMCCD, Andor iXon+ DU888 1k × 1k pixels; objective, Nikon Plan Fluor 100X oil objective plus 2.5X expander; lamp, Nikon C-HFGI) and a frame rate of 1 frame/min for 16 unique fields of view over 48 hours.

Cell Shape Analysis. The acquired phase-contrast images were processed with a pixel-based edge detection algorithm that applied a local smoothing filter, followed by a bottom-hat operation [1, 2]. The boundary of each cell was identified by thresholding the filtered image. A

† To whom correspondence may be addressed. Email: dinner@uchicago.edu or nfschere@uchicago.edu.

smoothing B-spline was interpolated through the boundary pixels to construct each cell contour. Each identified cell was then tracked over time to build a full time-trajectory. We chose to include only cells that divided for more than 10 generations in the analysis. A minimal amount of filtering was applied to each growth curve to remove spurious points (e.g., resulting from cells coming together and touching, or cells twisting out of plane). The timing of every division was manually checked, so the precision in determining this quantity results from the frame rate and not limitations of the automated analysis.

Synchronized Cell Wall Growth Assay. This material is complementary to that presented in Fig. 3 of the main text. *C. crescentus* cells from the strain NA1000 were grown in 15 mL of M2X liquid culture media from 24 hours at 30°C to an optical density at 600 nm of 0.4. The swarmer cells from this liquid culture were isolated using a modified protocol [3, 4]. To summarize, the culture was spun at 6000 rpm for 20 minutes at 4°C. The pellet was then resuspended in 1 mL of cold M2 media. The culture was then spun at 13000 rpm for 3 min at 4°C. The pellet was then resuspended in 900 μL of cold M2 media and 900 μL of Percoll. The culture was then spun at 11500 rpm for 20 min at 4°C, yielding two bands of cells. The upper band consisting of stalked cells was aspirated off, leaving the lower band of swarmer cells. The swarmer cells were then washed twice with 1 mL of M2 and spun at 11000 rpm for 3 min. The pellet was resuspended in 5 mL of M2X and 100 μL at a concentration of 1 mg/mL of fluorescent wheat germ agglutinin (flWGA), which had previously been shown to label the periphery of Gram-negative *E. coli* [5], was added to the resuspended culture and allowed to incubate with the cells for 10 min at 30°C to fully cover the cell wall. The culture was then diluted with 5 mL of M2X and grown in 30°C. 1 mL samples at 0, 20, 40, 60, 80, and 100 min were taken from the culture and frozen in dry ice. The cells were then fixed using 100 μL paraformaldehyde and washed with 100 μL phosphate buffered saline (PBS) and spun at 14000 rpm for 15 min. Microscope slides of the samples were made by combining 2 μL of sample, 2 μL of alginate, and 1 μL of 0.3 M Ca^{2+} to immobilize the cells.

Fluorescence images of the cells in the slides were obtained through confocal fluorescence microscopy (Supplementary Figure 11a). The fluorescence data was obtained by using ImageJ by creating midline profiles of the cells and integrating the fluorescence intensity along the midline (Supplementary Figure 11c). Supplementary Figure 11a shows that the fluorescence intensity is spatially uniform prior to constriction (i.e., for samples at $t < 40$ min), but the flWGA intensity patterns exhibit a pronounced minimum at the septum where the cell-wall is invaginated ($t > 60$ min). Supplementary Figure 11b presents deconvolution processed images obtained using the commercial software (Huygens). The deconvoluted single cell images more

clearly show the diminished flWGA label in the septal region. Moreover, the 100 min image even hints at secondary invaginations in a predivisional cell, consistent with our previous report on intergenerational continuity [2]. Supplementary Figure 11c shows the ensemble averaged normalized intensity profiles along the centerline axis of the cell at different time points. The spatial distribution of flWGA intensity suggests that growth is spatially uniform for $t < 40$ min and new cell-wall material is primarily synthesized at the invaginations for $t > 40$ min.

Supplementary Note 1

Size control models. The mixer model for size control (for $0 < t < \tau$) is defined by the following linear relationship between the size at birth, $l(0)$, and the size at division, $l(\tau)$,

$$l(\tau) = al(0) + \delta \ . \tag{S.1}$$

where τ is the division time. From this model, a sizer, a timer or an adder model can be recovered by considering appropriate limits for the slope and the intercept. A sizer is defined by $a = 0$, whereas an adder assumes a slope of unity, $a = 1$. In the timer limit we have $\delta = 0$.

From the plot of $l(\tau)$ vs $l(0)$ (Fig. 1b), we determine the parameters a and δ by a least-square linear fit to the scatter. For an adder model fit, we constrain the slope to unity and determine the added size, δ, from the intercept. Similarly, for the timer model fit, we determine the slope by assuming a zero intercept, as was done in Ref. [1]. To determine which of these models more accurately represent our data, we evaluate the deviation of the models from our data. In particular we evaluate the following quantities:

$$\Delta_{\text{mixer}} = [al(0) + \delta] - \langle l(\tau) \rangle \ ,$$

$$\Delta_{\text{adder}} = [l(0) + \delta] - \langle l(\tau) \rangle \ ,$$

$$\Delta_{\text{timer}} = [al(0)] - \langle l(\tau) \rangle \ ,$$

where the angular brackets mean ensemble average. As shown in Supplementary Figure 1A, $|\Delta_{\text{mixer}}| < |\Delta_{\text{adder}}| < |\Delta_{\text{timer}}|$. For initial cell sizes close to the ensemble mean $\langle l(0) \rangle$, all the models converge to $\langle l(\tau) \rangle$.

From the best fit parameters, a and δ, we can predict the relationship between the added size and the initial size,

$$\Delta l = (a - 1)l(0) + \delta \ ,$$

and also between $\kappa\tau$ and $l(0)$

$$\kappa\tau = \ln\left(a + \frac{\delta}{l(0)}\right),$$

without requiring any additional fitting parameters. (Figs. 1c, e). The corresponding deviations in Δl and $\kappa\tau$ from their mean values are given in Supplementary Figures 1 b-c.

Prior to the onset of constriction ($0 < t < t_c$), we use a relative timer model for size control, as evidenced by our data (Fig. 2). This is given by,

$$l(t_c) = al(0) + \delta'', \tag{S.2}$$

where a and δ'' are determined by fitting a straight line to the scatter plot of $l(t_c)$ vs $l(0)$. As a result, t_c is negatively correlated with $l(0)$ (Supplementary Figure 8a).

During cell-wall constriction phase ($t_c < t < \tau$), we use a pure adder model for size control, as evidenced by our data (Fig. 2). This is given by,

$$l(\tau) = l(t_c) + \delta', \tag{S.3}$$

where δ' is determined by fitting a straight line of unit slope to the scatter plot of $l(\tau)$ vs $l(t_c)$. As a result, $\tau - t_c$ is negatively correlated with $l(t_c)$, described by the relationship: $\tau - t_c = \kappa^{-1}\ln\left(1 + \delta'/l(t_c)\right)$ (Supplementary Figure 8b).

Supplementary Note 2

Crossover point determination from septal growth model (SGM). To determine the crossover point in the SGM, we implement the same procedure as we did for the experimental data. Specifically, we linearize the expression for $\ln\left(w_{\min}(t)/w_{\min}(0)\right)$ around $\kappa t \sim \epsilon$, which gives us,

$$\ln\left(w_{\min}(t)/w_{\min}(0)\right) \sim \ln\left(\sqrt{-\mu + 2\mu e^{\epsilon} - \mu e^{2\epsilon} + 1}\right) + \frac{\mu e^{\epsilon}\left(e^{\epsilon} - 1\right)(\kappa t - \epsilon)}{\mu - 2\mu e^{\epsilon} + \mu e^{2\epsilon} - 1} + \mathscr{O}[(\kappa t - \epsilon)^2], \tag{S.4}$$

where $\mu = (l_0/w_{\min}(0))^2$. We then determine the point of intersection, κt_c of the above linear expression evaluated at $\epsilon \sim 0.05$ (near the start of cell cycle) and at $\epsilon \sim 0.56$, which corresponds to near the end of the cell cycle since $\langle\kappa\tau\rangle = 0.56$. The dependence of κt_c on $l_0/w_{\min}(0)$ is shown in Fig. 4b-inset.

Supplementary Note 3

Mathematical model for crossover dynamics in cell wall growth. Here we explicitly model the crossover dynamics from lateral to septal cell wall growth, and compare the results

with our experimental data and the septal growth model (SGM) presented in the main text. To this end, we divide the midline axis of the cell in two parts - the septal region with length $l_s(t)$, and the lateral (non-septal) region with length $l_b(t)$ (Supplementary Figure 12a-inset). The growth model is defined by the following equations:

$$\begin{cases} dl_b/dt = \kappa l_b \Theta(t_c - t; \alpha) \ , \\ dl_s/dt = \kappa l_s + \kappa l_b \Theta(t - t_c; \alpha) \ , \end{cases} \tag{S.5}$$

where $\Theta(x;\alpha)$ is a continuous approximation of the Heaviside step function, $\Theta(x;\alpha) = 1/(1 + e^{-\alpha x})$, with α controlling the rate of the crossover to septal growth. The initial conditions are given by $l_b(0) = l(0)$, and $l_s(0) = 0$. Adding the two equations in (S.11) we recover exponential growth in total cell length, $dl/dt = \kappa l(t)$, where $l = l_b + l_s$.

If $\alpha \geq 1$ min^{-1}, the crossover from lateral to septal growth is sharp, such that for $t < t_c$, $dl_b/dt = \kappa l_b$, and $l_s = 0$. For $t > t_c$, $l_b(t) = l(t_c)$ and $dl_s(t)/dt = \kappa l_s + \kappa l_b(t_c)$ (Supplementary Figures 12a). We can identify the parameter v_0 in SGM (Eq. (2)) as $\kappa l_b(t_c)$. As the parameter α is reduced, the crossover dynamic becomes smooth, such that for $\alpha \ll 1$ min^{-1} the solution to Eq. (S.11) converges to the prediction by SGM (Supplementary Figure 12 c,d).

The data presented in Fig. 2 shows that $w_{\min}(t)$ continuously decreases from the start of the cell cycle in a biphasic manner. During the slow phase of constriction, i.e. for $t < t_c$, there is $\approx 10\%$ reduction in $w_{\min}$. Furthermore, our cell wall labelling experiments (Fig. 3) shows that cell wall growth is uniform for $t < t_c$ and septal growth becomes dominant for $t > t_c$. This indicates that septal growth is occurring from the beginning of the cell cycle and there is a smooth crossover from lateral to dominantly septal growth.

We treat α as a fitting parameter, determined by fitting the prediction of the crossover model with the experimental constriction data. Using elementary geometry (Fig. 4a), we have the relation,

$$w_{\min}(t) = w_{\min}(0)\sqrt{1 - (l_s(t)/w_{\min}(0))^2} \ , \tag{S.6}$$

which allows us to determine the minimum width from our model prediction for $l_s(t)$. As shown in Supplementary Figure 12b, for α closer to 1 min^{-1}, $w_{\min}$ is constant before $t < t_c$, in disagreement with our data. For small values of α, the prediction for $w_{\min}$ matches closely with our data. The best-fit value for the data presented in Supplementary Figure 12b is given by $\alpha = 0.001$ min^{-1}, which coincides with the constriction curve predicted by the SGM. In this limit the growth rate of l_b decreases linearly with $t_c - t$. The agreement between the SGM and the crossover model (in the limit $\alpha \ll 1$) is also evident from Supplementary Figures. 12c and d. These results justify that the SGM accurately describes constriction dynamics for the entire cell

cycle. Furthermore, the SGM predicts a crossover time for the biphasic constriction dynamics, without explicitly invoking the parameter t_c, as described below.

Supplementary Note 4

Comparing SGM with the experimental data. The SGM leads to the solution

$$l_s(t) = l_0(e^{\kappa t} - 1) \ , \tag{S.7}$$

where $l_0 = v_0\kappa$. Using the geometric relation, $w_{\min}(t) = \sqrt{w_{\min}(0)^2 - l_s(t)^2}$, we derive the time dependence of $w_{\min}$,

$$w_{\min}(t) = w_{\min}(0)\sqrt{1 - \left(l_0/w_{\min}(0)\right)^2 \left(e^{\kappa t} - 1\right)^2} \ . \tag{S.8}$$

Using Eq. (S.15), we can determine l_0 for each generation by fitting with the experimental data for $w_{\min}(t)$. The SGM also predicts the relation,

$$t = \kappa^{-1} \log\left(1 + \Delta w_{\min}(t)/l_0\right) \ , \tag{S.9}$$

where $\Delta w_{\min}(t) = \sqrt{w_{\min}(0)^2 - w_{\min}(t)^2}$. Setting $t = \tau$ and $w_{\min}(\tau) = 0$, we predict that cells with larger $w_{\min}(0)$ have a larger interdivision time. However, to compare with the experimental data presented in Fig. 4d, we set $w_{\min}(\tau) = w_{\min,\tau}$, which is the minimum width just prior to daughter cell separation. While naively one should expect $w_{\min}(\tau)$ to be zero, due to imaging limitations we don't observe any experimental data points below 0.4 μm. In Fig. 4d, we take $w_{\min,\tau} = \langle w_{\min}(t - \epsilon)\rangle$ where $\epsilon \approx 2$ min, and plot Eq. (3) against the experimental data.

Supplementary Note 5

Coupling of cell length and cell width. The cell lengths at birth and division are negatively correlated with $w_{\min}(0)$. This can be seen by combining Eq. (3) (SGM) and the mixer relationship: $l(\tau) = al(0) + \delta$. We obtain $w_{\min}(0) = l_0(a - 1 + \delta/l(0))$, from which follows the negative correlation between $w_{\min}(0)$ and $l(\tau)$. This is compared directly with the experimental data, as shown in Supplementary Fig. 13c.

As a consequence of the above relationship, we can directly derive the intergenerational variations in $w_{\min}(0)$ and describe the homeostasis in cell width. The cell length at birth in successive generations are related by: $l(0)^{i+1} = r(al(0)^i + \delta)$, where i is the generation index and r is the division ratio. $w_{\min}(0)$ values in successive generations are then related by:

$$w_{\min}(0)^{i+1} = \left(\frac{l_0}{r}\right)\left[1 + r - ar - \frac{a}{1 + w_{\min}(0)^i/l_0}\right] \ . \tag{S.10}$$

By substituting the values for a, δ, average r and l_0, we get:

$$w_{\min}(0)^{i+1} \approx 2.07 - \frac{2.27}{1 + w_{\min}(0)^i} \ . \tag{S.11}$$

We can solve the above equation in the limit of *homeostasis*, i.e. when the number of generations is large. Setting $w_{\min}(0)^{i+1} = w_{\min}(0)^i = \langle w_{\min}(0) \rangle$, one of the solutions to Eq. (S.18) is $\langle w_{\min}(0) \rangle = 0.811$ μm, which is in excellent agreement with the ensemble average value of $w_{\min}(0)$ from our experimental data 0.812 μm.

Supplementary Note 6

Consistency between the relative timer and the mixer model. The relative timer model implies that $\phi = t_c/\tau$ is independent of cell size at birth. Cell length at $t = t_c$ is related to the cell length at birth according to, $l(t_c) = l(0)e^{\kappa t_c} = l(0)e^{\kappa\tau\phi}$. The mixer model implies that, $\kappa\tau = \ln(a + \delta/l(0))$. Therefore, we get,

$$l(t_c) = l(0)(a + \delta/l(0))^{\phi} \ . \tag{S.12}$$

Linearizing $l(t_c)$ about $\langle l(0) \rangle$ then gives us a linear relationship between $l(t_c)$ and $l(0)$ (Fig. 2E), $l(t_c) = a_1 l(0) + \delta_1$, where

$$a_1 = (a\langle l(0) \rangle + \delta - \delta\phi)\,(a + \delta/\langle l(0) \rangle)^{\phi}\,/(a\langle l(0) \rangle + \delta) \ , \tag{S.13}$$

$$\delta_1 = \langle l(0) \rangle\,(a + \delta/\langle l(0) \rangle)^{\phi} - a_1\langle l(0) \rangle \ . \tag{S.14}$$

Plugging in $a = 1.25$, $\delta = 1.39$ μm and $\langle l(0) \rangle = 2.61$ μm, we get $a_1 = 1.17$ and $\delta_1 = 0.71$ μm, which is slightly different from the reported linear relationship in Fig. 2e. However, this discrepancy lies within the measurement error in $l(t_c)$, as shown below.

The discrepancy between the two estimates is given by: $|(1.25l(0)+0.43)-(1.17l(0)+0.71)| = |0.08l(0) - 0.28|$. Since $l(0)$ lies between $2-3$ μm, the range of discrepancy in $l(t_c)$ between the two estimates lies between $0.04-0.12$ μm, which is below the resolution of the optical microscopy images. Using $l(t_c) = l(0)e^{\kappa t_c}$, we get,

$$E[l(t_c)] = l(t_c)\sqrt{(E[l(0)]/l(0))^2 + (E[e^{\kappa t_c}]/e^{\kappa t_c})^2} \ , \tag{S.15}$$

where, $E[x]$ is the error in x. Next, we compute the error in determining $e^{\kappa t_c}$.

$$E[e^{\kappa t_c}] = e^{\kappa t_c} E[\kappa t_c] = e^{\kappa t_c}\sqrt{(E[\kappa]/\kappa)^2 + (E[t_c]/t_c)^2} \ . \tag{S.16}$$

Using $E[t_c] = 3$ min, $E[\kappa] = 0.0005$ min^{-1}, $E[l(0)] = 0.1$ μm, and the mean values for κ, t_c and $l(0)$, we get,

$$E[e^{\kappa t_c}] = 0.37\sqrt{(0.0005/0.008)^2 + (3/47)^2} = 0.37\sqrt{0.008} = 0.03 \ . \tag{S.17}$$

Therefore,

$$E[l(t_c)] = \langle l(t_c)\rangle \sqrt{(0.1/2.61)^2 + (0.03/0.37)^2} = 3.72\sqrt{0.008} = 0.33\ \mu\text{m}\ . \qquad \text{(S.18)}$$

Hence, the measurement error in $l(t_c)$ is 0.33 μm, which is more than the discrepancy between the two estimates for $l(t_c)$.

Supplementary Discussion

Within the mixer model, a cell grows until it reaches a target size $l(\tau) = al(0) + \delta$, which leads to the division time given by Eq. (1). Therefore a newborn cell already knows the division time and division size by virtue of the mixer model strategy. In phase 1 (slow constriction phase), growth occurs until the difference of the current cell size from its target size approximately equals the size of the daughter poles. Phase 1 terminates when the cell size reaches the value $l(t_c) = al(0) + \delta'$, which is coincident with the relative time rule $t_c \approx 0.6\tau$. Within measurement error, there is no contradiction between the relative timer and the mixer rule, as shown by our error analysis. In phase 2 (fast constriction phase), a cell grows by adding a constant size, $\delta'' = \delta - \delta'$. The time from septation to division is thus given by the amount of time taken to add δ'', equivalent to the size of the daughter cell poles (Fig. 4; Supplementary Figure 8). Together, phase 1 and phase 2 add to the mixer model for the entire cell cycle.

A potential mechanism for triggering septation could be similar to the recent model proposed by Harris and Theriot [6]. For instance, cells could accumulate precursor molecules for peptidoglycan synthesis proportional to its growing size. While some of these peptidoglycan precursors will be used to make lateral cell wall, there will be an excess amount of unused precursor molecules accumulated. Septation will be triggered when this excess of unused peptidoglycan precursors is roughly equivalent in mass to the material needed for synthesizing new daughter cell poles.

The biphasic growth behavior is accounted for by the septal growth model (SGM) as evident in Fig. 4b. The SGM leads to a prediction for the crossover time, as analytically derived in the previous section and shown by the inset to Fig. 4b. Although the data in Fig. 2a shows biphasic dynamics for the minimum width, there is noticeable constriction for $t < t_c$. This indicates that septation begins slowly from cell birth, otherwise $w_{\min}(t)$ would be constant for $t < t_c$. Indeed, our cell-wall labeling experiments show that growth is uniform for $t < t_c$ and dominantly septal for $t > t_c$ (Fig. 3). Based on our WGA labeling data we cannot conclude that there is a sharp switch from lateral to septal growth, but a smooth transition from uniform growth to dominantly septal growth, which is reproduced by the SGM (Supplementary Figure

12). It is clear that growth cannot be purely septal during the stalked cell cycle, otherwise the added cell size will be directly proportional to the cell width.

The SGM is also consistent with the relative timer model, which is quantified by the scaling of t_c vs τ. This is a direct consequence of the scaling relation predicted by SGM: $\kappa t_c = 0.37$ (Fig. 4b-inset) and the relation: $\tau = \kappa^{-1} \ln(1 + w_{\min}(0)/l_0)$. Substiuting $\kappa = 0.37 t_c^{-1}$ in the equation for τ we obtain: $t_c = 0.37\tau / \ln(1 + w_{\min}(0)/l_0)$. Using the average values $w_{\min}(0) = 0.8$ μm and $l_0 = 1$ μm, we obtain $t_c = 0.63\tau$ which is the result of the relative timer model.

Supplementary References

[1] S. Iyer-Biswas, C. S. Wright, J. T. Henry, K. Lo, S. Burov, Y. Lin, G. E. Crooks, S. Crosson, A. R. Dinner, and N. F. Scherer, Proceedings of the National Academy of Sciences **111**, 15912 (2014).

[2] C. S. Wright, S. Banerjee, S. Iyer-Biswas, S. Crosson, A. R. Dinner, and N. F. Scherer, Scientific Reports **5**, 9155 (2015).

[3] M. Evinger and N. Agabian, Proceedings of the National Academy of Sciences **76**, 175 (1979).

[4] M. E. Marks, C. M. Castro-Rojas, C. Teiling, L. Du, V. Kapatral, T. L. Walunas, and S. Crosson, Journal of Bacteriology **192**, 3678 (2010).

[5] T. S. Ursell, J. Nguyen, R. D. Monds, A. Colavin, G. Billings, N. Ouzounov, Z. Gitai, J. W. Shaevitz, and K. C. Huang, Proceedings of the National Academy of Sciences **111**, E1025 (2014).

[6] L. K. Harris and J. A. Theriot, Cell **165**, 1479 (2016).

[7] D. Ratkowsky, J. Olley, T. McMeekin, and A. Ball, Journal of Bacteriology **149**, 1 (1982).

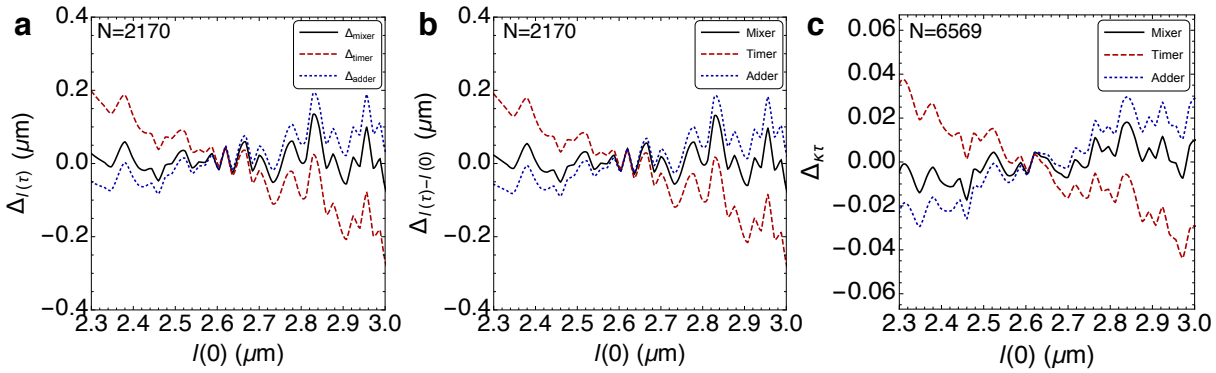

Supplementary Figure 1. **Errors in size control models**. Deviation about the mean for the **a.** final length $l(\tau)$, **b.** added length, $l(\tau) - l(0)$ and the **c.** normalized cell cycle time, $\kappa\tau$, as given by a mixer (solid curve), adder (dotted curve) and a timer model (dashed curve).

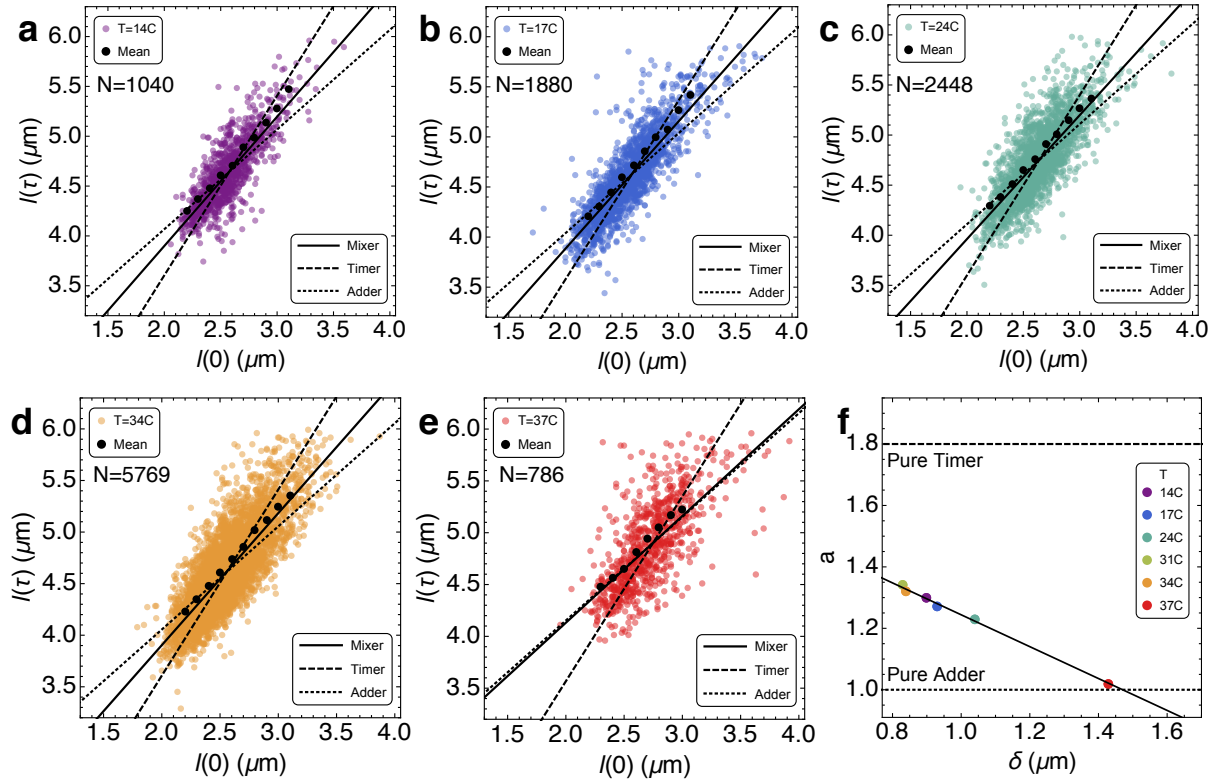

Supplementary Figure 2. **Cell size regulation at various temperatures. a-e.** Correlation between the cell size at division, $l(\tau)$, and the cell size at birth, $l(0)$, at various temperatures. Black solid line represents a least square linear fit to the data (mixer model). Corresponding fits by timer and adder models are given by dashed and dotted lines, respectively. The solid circles represent mean data binned in $l(0)$. **f.** Slope (a) and intercept (δ) of the mixer model, $A(\tau) = aA(0) + \delta$ where A is the cell area, as a function of temperature. With increasing temperature, cells approach the adder model of size control with $a \to 1$. Solid line is a least square linear fit, $a = -0.5\delta + 1.73$.

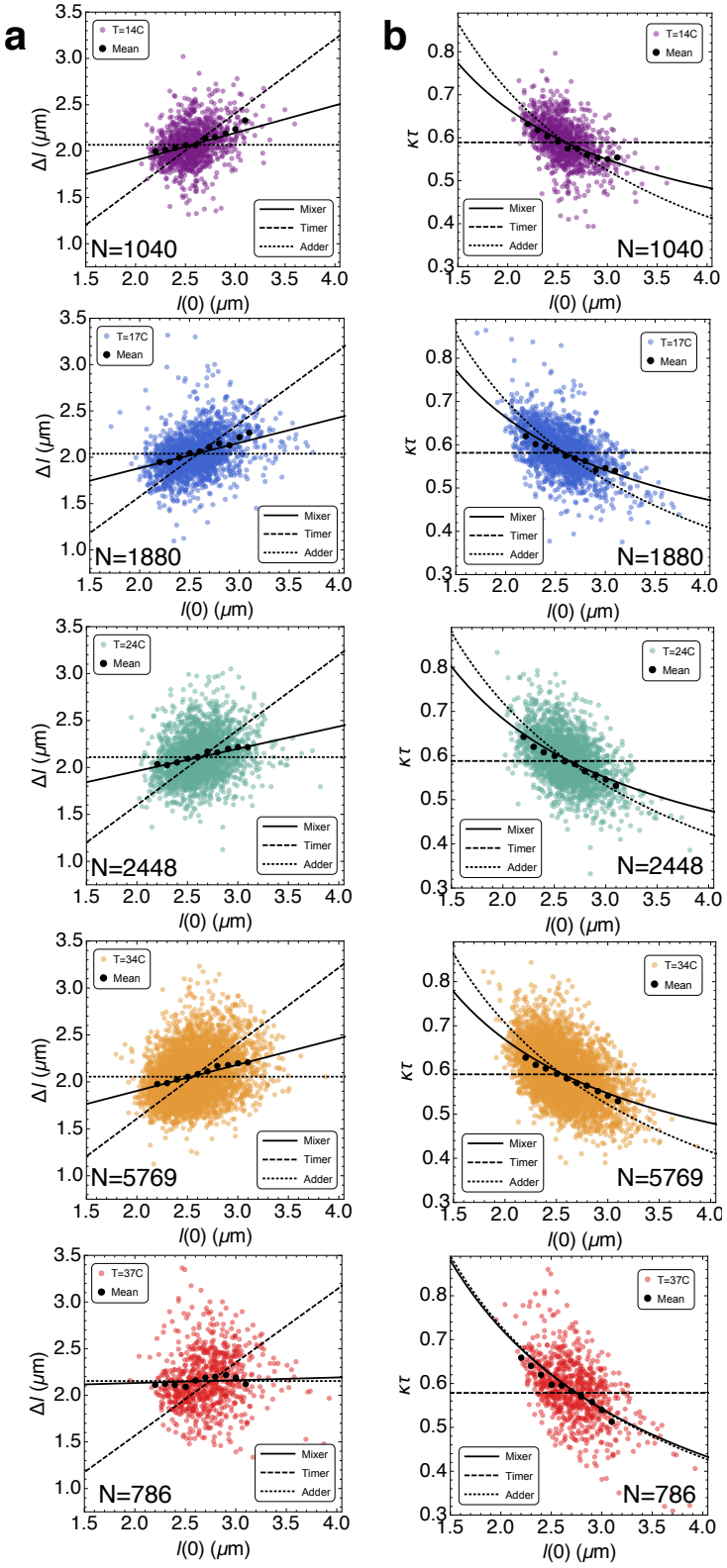

Supplementary Figure 3. **Control of added size and division times at various temperatures.** **a.** Correlation between the added size, $\Delta l = l(\tau) - l(0)$, and the cell size at birth, $l(0)$, at various temperatures. **b.** (Negative) Correlation between the normalized cell cycle duration, $\kappa\tau$), and the cell size at birth, $l(0)$, at various temperatures. Black solid line represents a least square linear fit using the mixer model. Corresponding fits by timer and adder models are given by dashed and dotted lines. respectively. The solid circles represent mean data binned in $l(0)$.

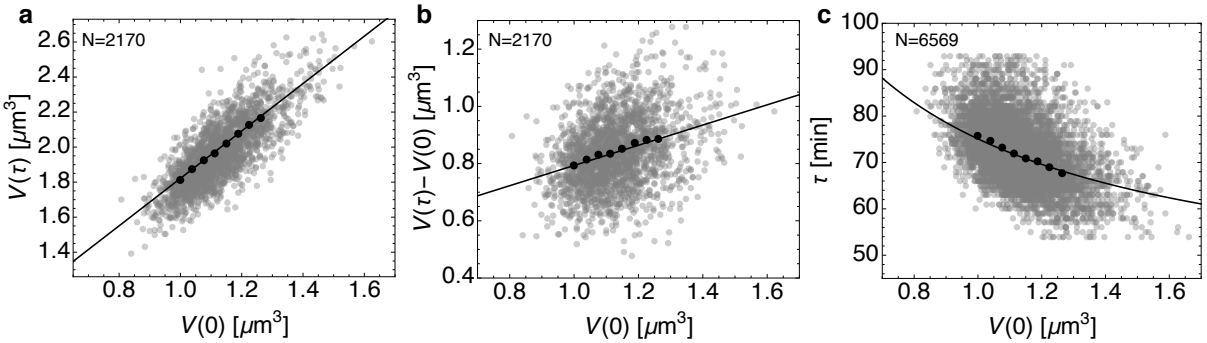

Supplementary Figure 4. **Volume data supports mixer model. a.** Correlation between cell volume at birth and cell volume at division is supported by the mixer model: $V(\tau) = 1.35V(0)+0.45$ (solid curve). Solid circles represent mean data binned in $V(0)$. Cell volume is estimated from measurements of cell midline length and width, assuming a circular cross-section. **b.** Positive correlation between the added volume and the cell volume at birth. **c.** Negative correlation between the division time and $V(0)$.

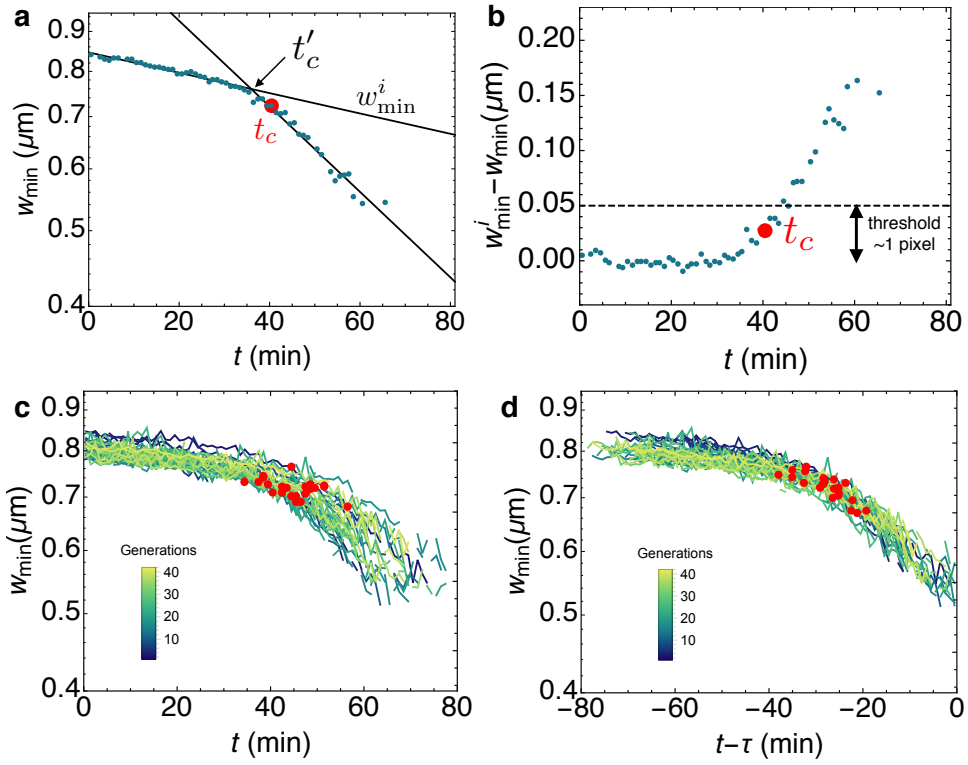

Supplementary Figure 5. **Determination of crossover time. a.** Fitting the data for $w_{\min}$ with a piecewise exponential decay. Initial phase of decay is labeled $w^i_{\min}$ and the point of interesection occurs at t'_c. **b.** Crossover time or constriction initiation time, t_c, is estimated to occur 3 frames prior to $w^i_{\min} - w_{\min}$ crossing the threshold 0.05 μm. The green dots are data for a representative generation. **c.** Dynamics of $w_{\min}$ vs t for a representative cell in semi-log scale. Red solid circles indicate crossover point t_c. **d.** Dynamics of $w_{\min}$ vs $t - \tau$ in semi-log scale for a representative cell, same as in **b**. Curves collapse although location of t_c is spread out.

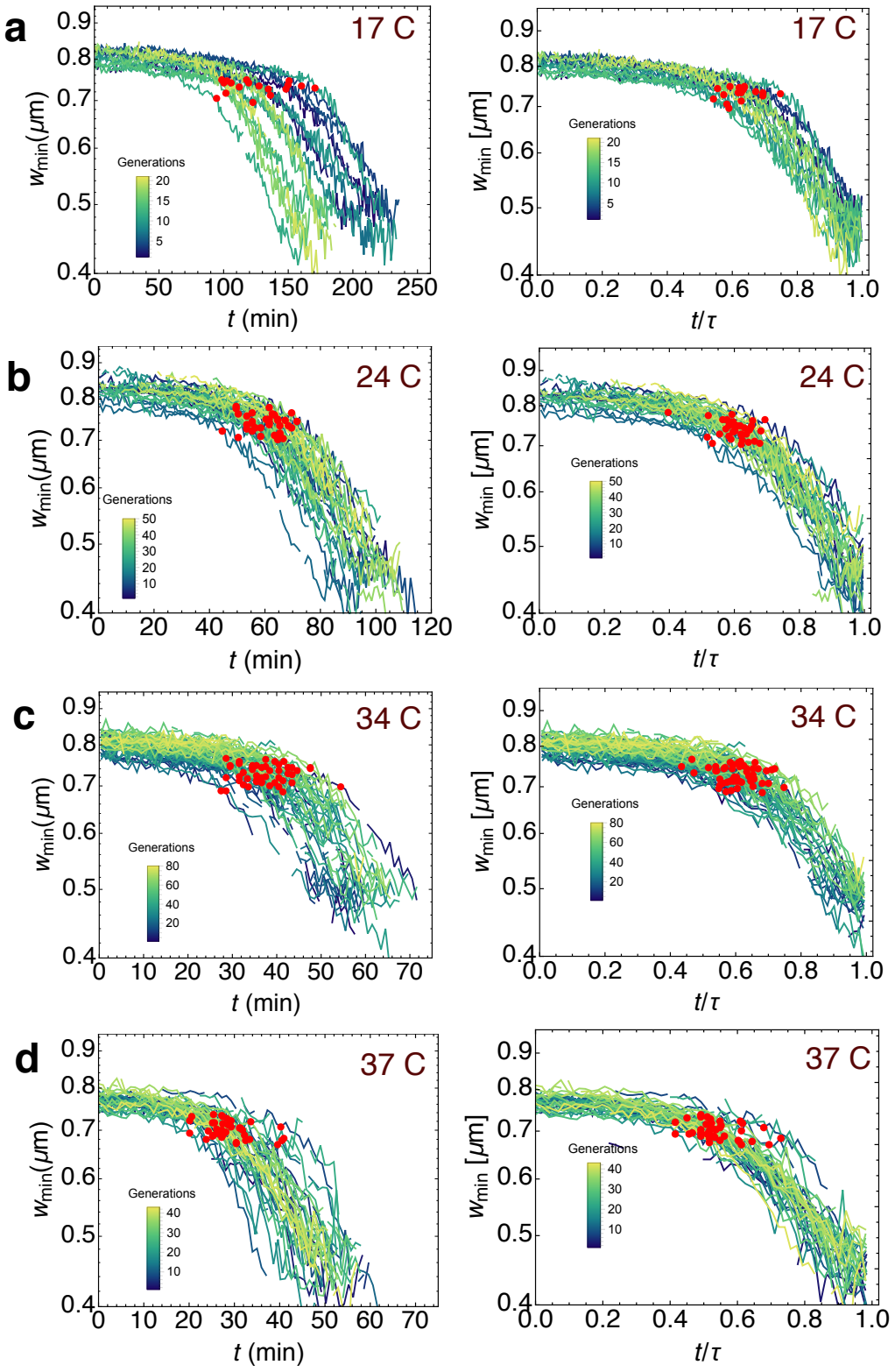

Supplementary Figure 6. **Crossover dynamics at various temperatures.** Dynamics of constriction ($w_{\min}(t)$) for a representative cell across all generations for temperatures equal to: **a,** 17C **b,** 24C **c,** 34C and **d,** 37C. Locations of the crossover (red) are much better aligned when the constriction curves are plotted vs relative time (right column) as opposed to absolute time (left column).

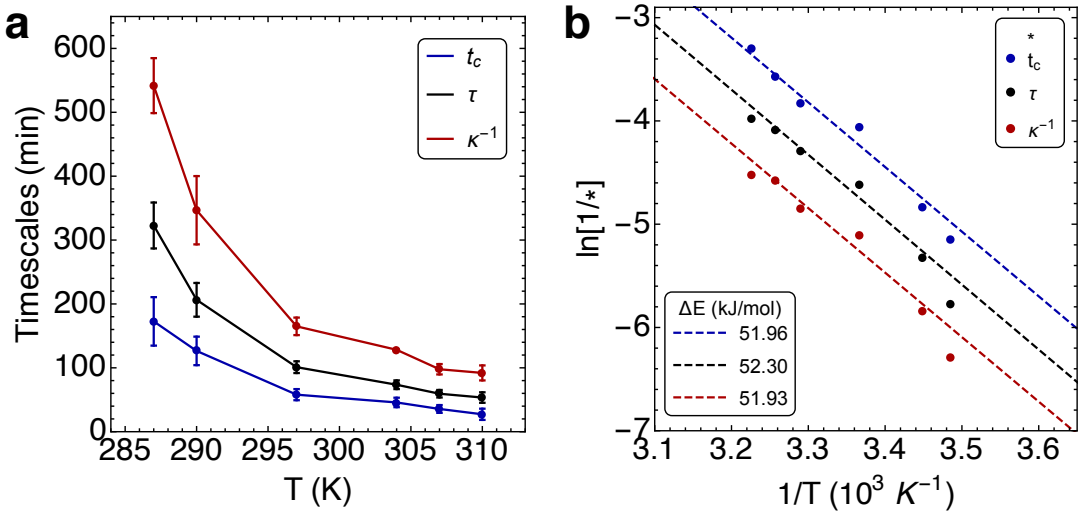

Supplementary Figure 7. **Temperature variations of the crossover time. a.** The timescales t_c, τ and κ^{-1} monotonically decrease with increasing temperature. Error bars reprsent ± 1 standard deviation. **b.** Arrhenius plot for the variations of t_c, τ and κ^{-1} with temperature. We estimate the effective activation energy for crossing t_c to be approximately equal to the activation barrier for τ and κ^{-1}, $\Delta E \simeq 52$ kJ/mol. The estimate for ΔE comes from the slope of the dashed lines that are given by the Arrhenius equation: $\theta = \theta_0 e^{-\Delta E/k_B T}$, where θ represents κ, τ^{-1} and t_c^{-1}. We fit the Arrhenius equation in the temperature range: 14°C-37°C. The expected deviations from Arrhenius behavior are noticable at the extremes of the temperature range [7].

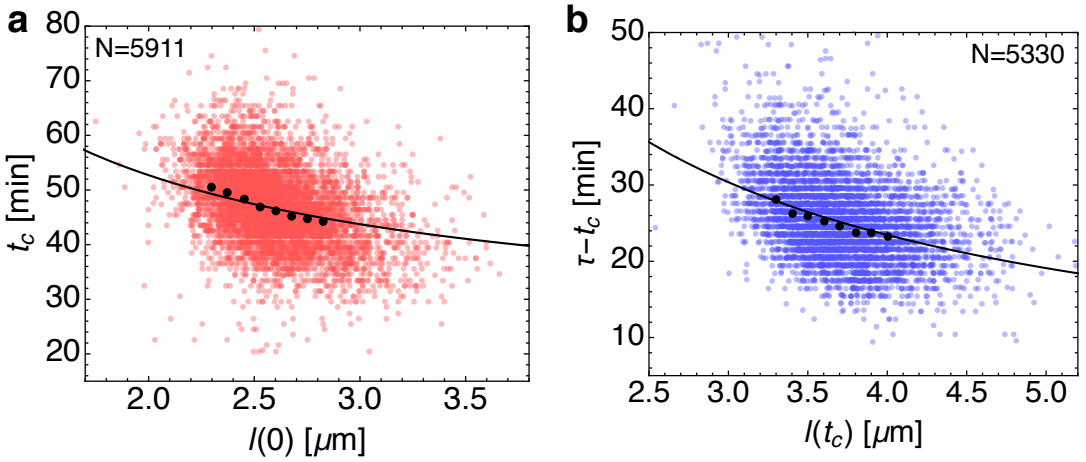

Supplementary Figure 8. **Preconstriction and post-constriction times are negatively correlated with cell size. a.** Negative correlation between the crossover time and cell length at birth, consistent with a mixer model (solid curve). **b.** Negative correlation between post-constriction time and cell length at t_c, consistent with a pure adder model (solid line). Solid circles represent mean data binned in cell length.

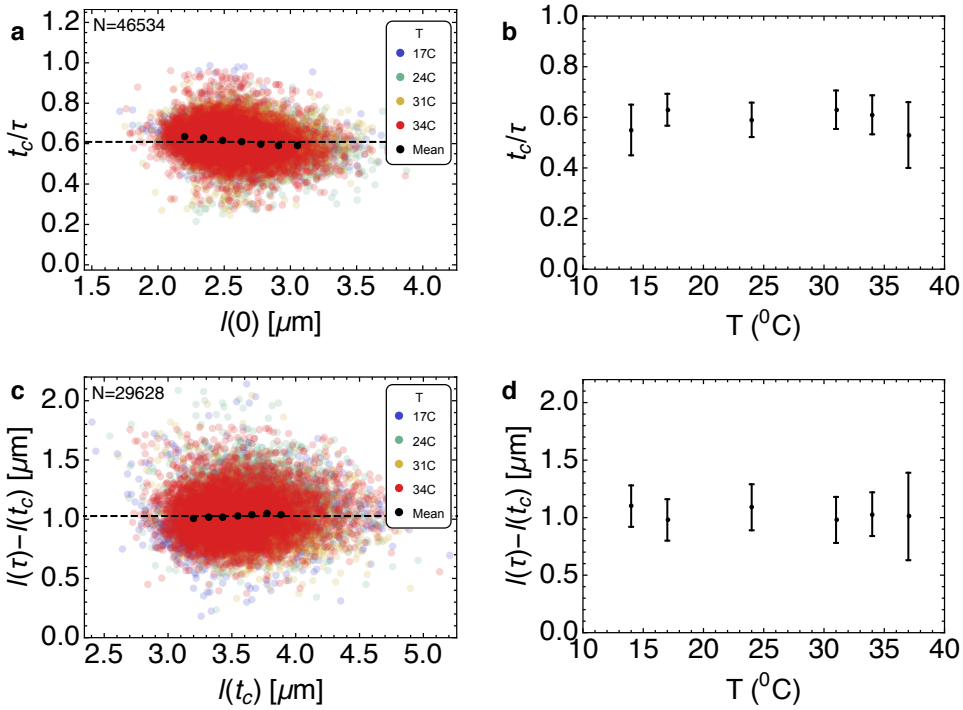

Supplementary Figure 9. **Relative timer to adder crossover at the onset of constriction at different temperatures. a.** Relative crossover time, t_c/τ, is uncorrelated with the cell length at birth at all temperatures. Dashed line is the mean value for t_c/τ ($= 0.6$) for all temperatures. **b.** t_c/τ does not vary with changing temperature of the medium. Solid circles represent ensemble mean and error bars indicate ± 1 standard deviation. **c.** Added length after constriction is uncorrelated with $l(t_c)$ at all temperatures, thus supporting a pure adder phase post constriction. Mean added size is 1.03 μm (Dashed line). **d.** Post constriction added length does not vary with temperature. Solid circles represent ensemble mean and error bars indicate ± 1 standard deviation.

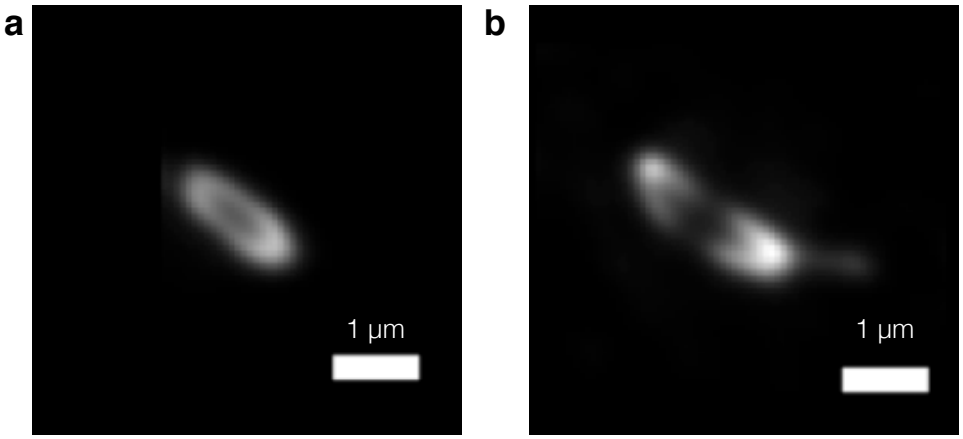

Supplementary Figure 10. **WGA labels the cell-wall of *C. crescentus* cells.** *C. crescentus* stalked cells coated with WGA fixed after 0 min (**a**) and 80 min (**b**) of growth. The middle plane of the confocal stack is shown after deconvolution for a representative cell. The mid-cell focal plane shows enhanced fluorescence from the perimeter, demonstrating that flWGA marks the peripheral cell wall.

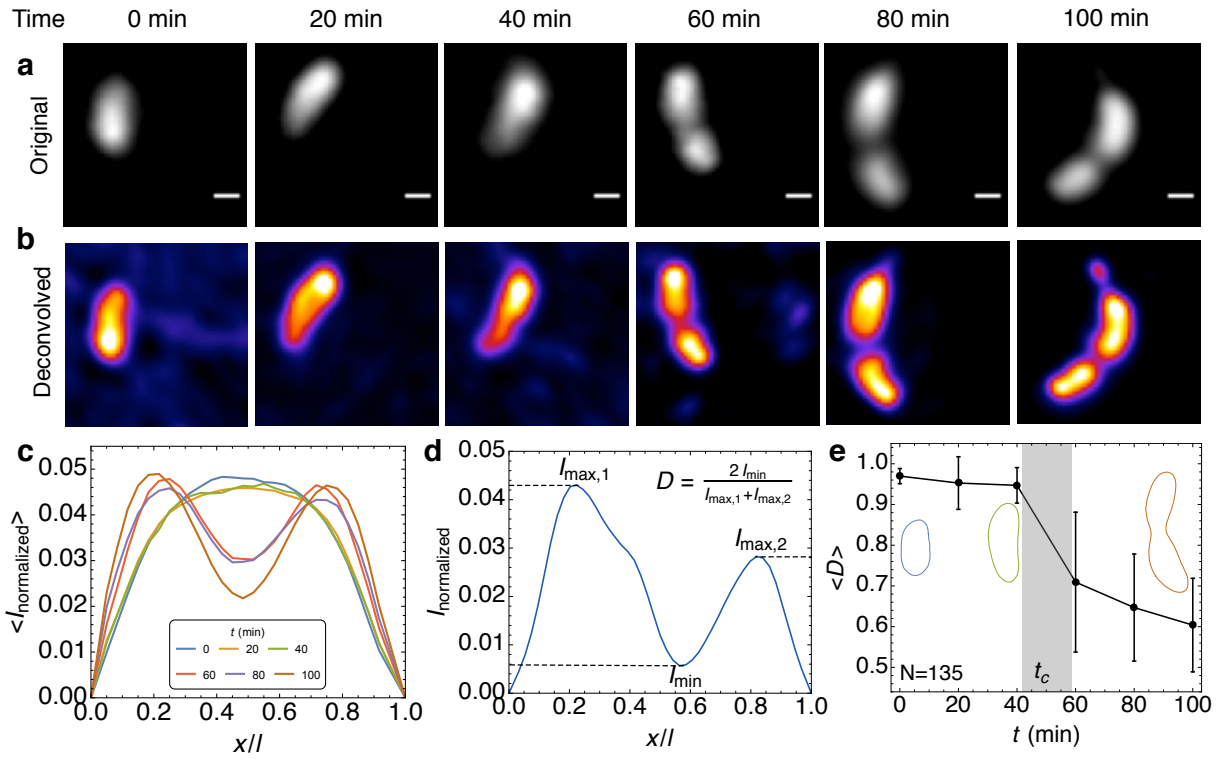

Supplementary Figure 11. **Crossover in cell wall growth dynamics at the onset of constriction**. **a.** Confocal fluorescent images of a representative *C. crescentus* cell labeled with fluorescent WGA taken after 0, 20, 40, 60, 80 and 100 min of growth in culture medium. The scale bars represent 0.5 μm. **b.** Shows the same data but deconvoluted using the Huygens software package. The depletion of fluorescence reveals the underlying spatial pattern of growth, i.e. growth occurs where the fluorescence is minimized. **c.** Ensemble averaged spatial distribution of normalized flWGA intensity along the centerline axis of the representative cell in (**a**) and (**b**) at t =0, 20, 40, 60, 80 and 100 min. The arc length along centerline, x, is normalized by the cell length, l. **d.** A typical intensity profile is characterized by one minimum at the septum ($I_{\rm min}$) and two maxima near either pole ($I_{\rm max,1}$, $I_{\rm max,2}$). We define the index of uniformity of cell wall growth as, $D = 2I_{\rm min}/(I_{\rm max,1} + I_{\rm max,2})$. **e.** Ensemble averaged dynamics of the growth uniformity index ($\langle D \rangle$) reveal a crossover from uniform growth ($\langle D \rangle \simeq 1$) to localized septal growth between 40 to 60 min (shaded area). Error bars indicate ± 1 standard deviation. The inset shows representative splined cell contours.

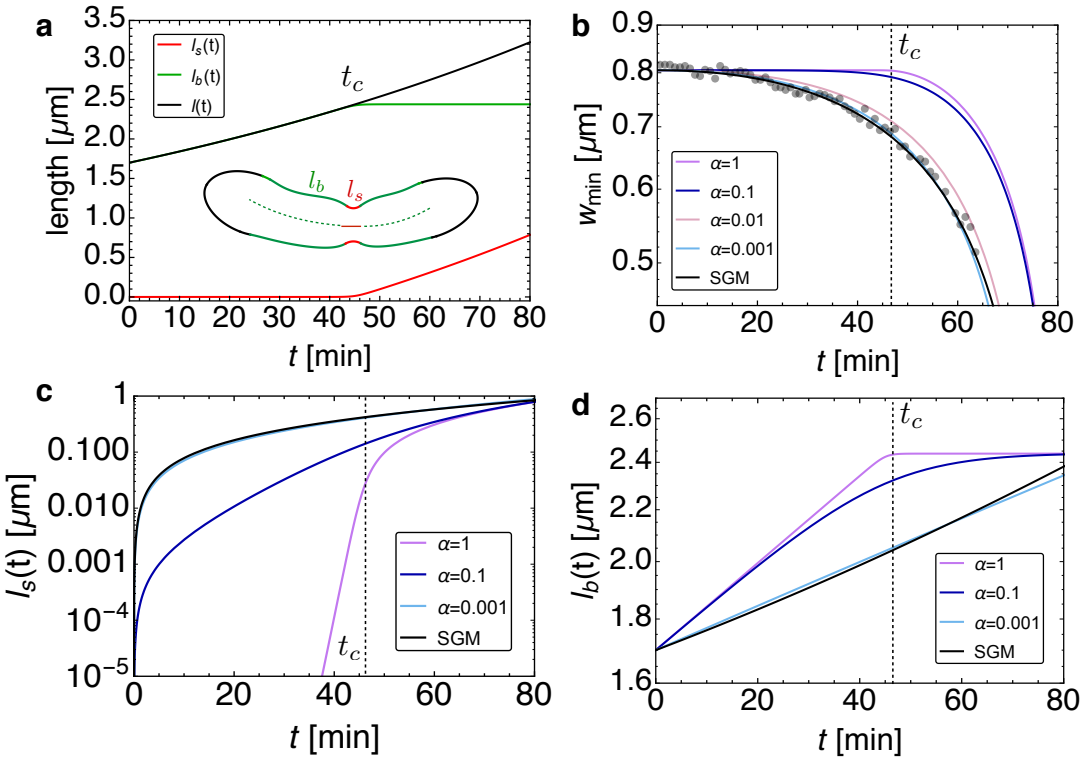

Supplementary Figure 12. **Model for crossover from lateral to septal growth. a.** Dynamics of total cell length (black), septal length, l_s (red), and the lateral length, l_b vs time for $\alpha = 1$ min^{-1} using model (S.11). Inset: Caulobacter cell contour showing the septal and the lateral midline lengths. **b.** Comparison of the crossover model (Eq. (S.11), for varying α) and the septal growth model (SGM, black line) with the experimental data for $w_{\min}$ for a representative cell generation (Gray solid circles). **c.** Dynamics of $l_s(t)$ predicted by the crossover model (varying α) and SGM (black). **d.** Dynamics of $l_b(t)$ predicted by the crossover model (varying α) and SGM (black). In (**b-d**) $\alpha = 0.001$ min^{-1} (green curve) overlaps with the SGM (black curve).

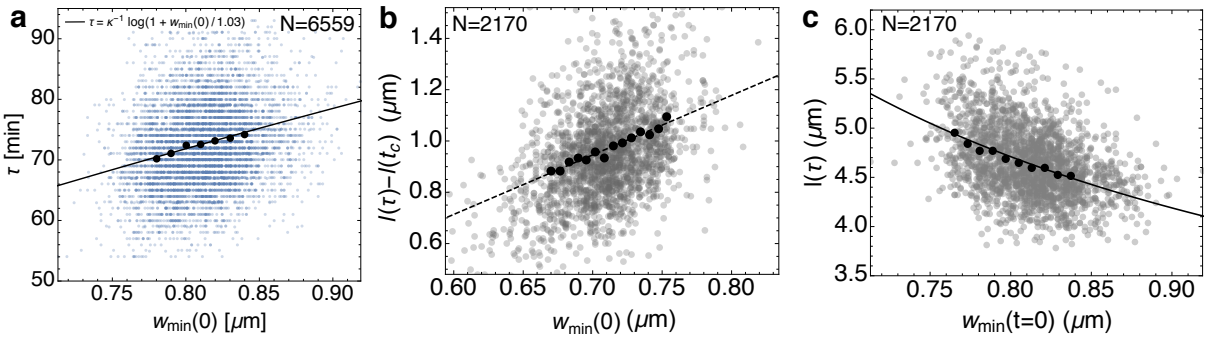

Supplementary Figure 13. **Cell shape controls cell size. a.** Correlation between division time (τ) and $w_{\min}(0)$. The black dots represent mean data binned in $w_{\min}(0)$ and the solid line is Eq. (3). **b.** Correlation between $l(\tau) - l(t_c)$ and the septal width $w_{\min}(t_c)$. The solid circles represent mean data binned in $w_{\min}(t_c)$ and the dashed line is a linear fit to the scatter. **c.** Negative correlation between final cell size, $l(\tau)$, and the initial septal width, $w_{\min}(0)$. The binned data are in solid circles; whereas the prediction of the septal growth model, $l(\tau) = \delta\left(1 - \frac{a}{1+\Delta w_{\min}/l_0}\right)^{-1}$, is given by the solid line.